Available online at ScienceDirect

Nuclear Engineering and Technology

journal homepage: www.elsevier.com/locate/net

Original Article

Mass Transfer Experiments for the Heat Load During In-Vessel Retention of Core Melt

*Hae-Kyun Park and Bum-Jin Chung**

Department of Nuclear Engineering, Kyung Hee University, 1732 Deokgyoung-daero, Giheung-gu, Yongin-si, Gyeonggi-do 17104, Republic of Korea

ARTICLE INFO

Article history:
Received 7 November 2015
Received in revised form
14 January 2016
Accepted 10 February 2016
Available online 11 March 2016

Keywords:
Hemisphere
In-Vessel Retention
Mass Transfer
Natural Convection
Oxide Pool
Volumetric Heat Source

ABSTRACT

We investigated the heat load imposed on the lower head of a reactor vessel by the natural convection of the oxide pool in a severe accident. Mass transfer experiments using a $CuSO_4$ $-H_2SO_4$ electroplating system were performed based on the analogy between heat and mass transfer. The Ra'_H of 10^{14} order was achieved with a facility height of only 0.1 m. Three different volumetric heat sources were compared; two had identical configurations to those previously reported, and the other was designed by the authors. The measured *Nu*'s of the lower head were about 30% lower than those previously reported. The measured angular heat flux ratios were similar to those reported in existing studies except for the peaks appearing near the top. The volumetric heat sources did not affect the *Nu* of the lower head but affected the *Nu* of the top plate by obstructing the rising flow from the bottom.

1. Introduction

Nuclear fuels may melt and relocate in the lower head of a reactor vessel in a hypothetical severe accident. Owing to the density difference, the core melt stratifies into an oxide pool and a metal layer. The decay heat generated from the oxide pool is transferred to the reactor vessel and the upper metal layer by natural convection. In an IVR (in-vessel retention) strategy, the outside of the reactor vessel is filled with water and is cooled by natural convection. It is a crucial issue whether the reactor vessel can be cooled sufficiently to maintain physical integrity and contain the core melt.

Many studies have investigated the heat load to a reactor vessel from the natural convection of the oxide pool and metal layer, as well as external reactor vessel cooling (ERVC); however, the unknown material properties of the core melt and the tough experimental conditions, which include large buoyancy, make these measurements difficult. Additionally, the self-exothermic characteristics and large buoyancy of the oxide pool have limited the research on this topic. Volumetric

* *Corresponding author.*
E-mail address: bjchung@khu.ac.kr (B.-J. Chung).
http://dx.doi.org/10.1016/j.net.2016.02.015

heating simulations have been performed using various heating/cooling methods (e.g., microwave heating, Joule heating using various shapes of wire electrodes, and outside cooling for preheated working fluids); however, the reported range of Ra'_H varies.

In this study, natural convection experiments were performed on an oxide pool. A mass transfer experiment replaced the heat transfer experiment based on the analogy between heat and mass transfer. The $CuSO_4$–H_2SO_4 electroplating system was used as the mass transfer system, and three different volumetric heat sources, which were proposed in previous studies or by the current study, were compared.

2. Previous studies

Bonnet and Seiler [1] investigated natural convection heat transfer from an oxide pool using a two-dimensional (2D) semicircular experimental facility (BALI). They used direct Joule heating via a lattice-shaped electrode wire to simulate the volumetric heat source. The range of Ra'_H was from 10^{15} to 10^{17}. Water was used as the working fluid, and isothermal cooling conditions were established using coolant circulation outside the pool. Two conditions, cooling and insulating, were used for the top plate. The heat flux measured along the pool curvature was minimum at the pool bottom and increased gradually moving from the bottom to the top in all cases. However, the shape of the heat flux curves depended on the top plate cooling conditions: convex upward for a cooled top and convex downward for an insulated top. The heat transfer correlations for the top plate (Nu_{up}) and bottom hemisphere (Nu_{dn}) are given below:

$$Nu_{up} = 0.383\, Ra_H'^{0.233} \tag{1}$$

and

$$Nu_{dn} = 0.116\, Ra_H'^{0.25} \tag{2}$$

Kymalainen et al. [2] simulated natural convection heat transfer from the oxide pool of the Loviisa nuclear power plant in Finland using a 2D torispherical facility (COPO I). The volumetric heat source was simulated by direct Joule heating using horizontal wire electrodes. Ra'_H ranged from 1.24×10^{14} to 1.61×10^{15}, with $ZnSO_4$–H_2O as the working fluid. Dozens of cooling units were attached to the outside of the facility to establish isothermal cooling conditions. Nu_{dn} was minimum at the bottom and increased gradually as the angle measured from the center of the torisphere increased.

Sehgal et al. [3] investigated the phenomena using a 2D semicircular facility, Simulation of In-vessel MElt COolability (SIMECO). They used horizontal wire electrodes to simulate the volumetric heat source as in the COPO I study [2]. Water and $NaNO_3$–KNO_3 were used as working fluids to achieve Ra'_H values of 3.14×10^{13} and 1.51×10^{13}, respectively. Isothermal inner wall conditions were established by coolant circulation. The heat flux increased with the angle measured from the bottom of the vessel. The maximum heat flux occurred at about 80°, then the heat flux decreased toward the top of the vessel.

Lee et al. [4] investigated the same phenomena using a 2D semicircular facility, Simulation of Internal Gravity-driven Melt Accumulation Circular Pool (SIGMA CP). The Ra'_H ranged from 5.71×10^6 to 7.04×10^{11} using water and air as the working fluids. Direct Joule heating with bent wire electrodes (S-bend) was used to simulate the volumetric heat source. Heat fluxes at the top plate and lower head were measured. The heat flux of the lower head increased with the angle; the maximum value was observed between 80° and 90°. However, the heat flux values at the top plate depended on the position. Heat transfer correlations were developed for the top plate (Nu_{up}) and lower head (Nu_{dn}), as given below:

$$Nu_{up} = 0.31\left(Ra'_H Pr^{-0.36}\right)^{0.245} \tag{3}$$

and

$$Nu_{dn} = 0.219\left(Ra'_H Pr^{-0.215}\right)^{0.235}. \tag{4}$$

Suh et al. [5] performed heat transfer experiments using a three-dimensional (3D) facility, Simulation of Internal Gravity-driven Melt Accumulation 3-Dimensional (SIGMA 3D). The working fluids and volumetric heat source were identical to those of the SIGMA CP study [4]. Ra'_H values ranged from 4.46×10^6 to 3.5×10^{10}. The heat flux distributions at the top plate and the lower head were similar to those of SIGMA CP [4].

Palagin and Kretzschmar [6] investigated heat transfer using the 3D Late In-Vessel phase Experiments (LIVE) facility. The working fluid was water. Direct Joule heating was applied using arrays of ring-shaped wire electrodes to simulate the volumetric heat source. The Ra'_H value was 1.2×10^{14}. The heat flux at the top plate and the heat flux of the lower head above 77° were not measured, as the working fluid did not completely fill the facility. The heat flux gradually increased as the angle from the bottom increased.

Asfia and Dhir [7] studied natural convection heat transfer using a 3D facility [University of California, Los Angeles (UCLA), Los Angeles, CA, USA]. Freon-113 was used as the working fluid, which was heated by microwaves. Cooling and insulating conditions were established for the top plate, which resulted in Ra'_H ranges of 5×10^{11}–8×10^{13} and 4.7×10^{11}–7.8×10^{13}, respectively. The heat flux increased with the angle measured from the bottom but dropped near the top plate in all cases. The peak heat flux for the insulated top was measured at a higher location (larger angle) than that for the cooled top.

Theofanous et al. [8] conducted an experiment using the 3D ACOPO facility. Preheated water was used as the volumetrically heated working fluid. Ra'_H values ranged from 1×10^{14} to 2×10^{16}. Five and 10 cooling units were attached to the upper and lower heads, respectively, to establish isothermal conditions. Nu_{dn} increased with the angle, as measured from the bottom. The heat transfer correlations used to describe the process are as follows:

$$Nu_{up} = 1.95 Ra_H'^{0.18} \tag{5}$$

and

$$Nu_{dn} = 0.3 Ra_H'^{0.22}. \tag{6}$$

3. Materials and methods

3.1. Methodology

Heat and mass transfer systems are analogous as the mathematical models describing the two phenomena are of the same form [9]. Therefore, although the two phenomena are different in nature, they can be treated mathematically as the same. Table 1 summarizes the governing parameters for heat and mass transfer systems. In this study, measurements were made using a copper sulfate–sulfuric acid ($CuSO_4$–H_2SO_4) electroplating system as the mass transfer system. This technique was developed by several researchers [10–13], and the methodology is well established [14–21]. The physical properties were calculated using Eqs. (7–14) by Fenech and Tobias [13], which are accurate within ± 0.5% at 20–22°C. Compared with temperature measurements, this technique is attractive as it provides a simple, low-cost, accurate method of measurement through electric current measurement [22,23].

$$\rho(\mathrm{kg/m^3}) = \left(0.9978 + 0.06406C_{H_2SO_4} - 0.00167C_{H_2SO_4}^2 + 0.12755C_{CuSO_4} + 0.01820C_{CuSO_4}^2\right) \times 10^3, \quad (7)$$

$$\mu(cp) = 0.974 + 0.1235C_{H_2SO_4} + 0.0556C_{H_2SO_4}^2 + 0.5344C_{CuSO_4} + 0.5356C_{CuSO_4}^2, \quad (8)$$

$$\mu D_m(\mathrm{m^2/s}) = \left(0.7633 + 0.00511C_{H_2SO_4} + 0.02044C_{CuSO_4}\right) \times 10, \quad (9)$$

$$t_{Cu^{2+}} = \left(0.2633 - 0.1020C_{H_2SO_4}\right) \times C_{CuSO_4}, \quad (10)$$

$$\Delta\rho/\rho = C_{CuSO_4}\left[\beta_{CuSO_4} - \beta_{H_2SO_4}\left(\Delta C_{H_2SO_4}/\Delta C_{CuSO_4}\right)\right], \quad (11)$$

$$\Delta C_{H_2SO_4}/\Delta C_{CuSO_4} = -0.000215 + 0.113075\gamma^{1/3} + 0.85576\gamma^{2/3} - 0.50496\gamma, \quad (12)$$

where

$$\gamma = C_{CuSO_4}/\left(C_{CuSO_4} + C_{H_2SO_4}\right). \quad (13)$$

and

$$\beta_j = 1/\rho\left[\partial\rho/\partial C_j\right]_{T,C_{k\neq j}}. \quad (14)$$

In the electroplating system, cupric ions are reduced at the cathode surface. The resulting decrease in the cupric ion concentration in the solution induces a buoyant force. Thus, the cathode is used as the hot wall. To minimize cupric ion migration, sulfuric acid is added as the supporting electrolyte to increase the electric conductivity of the solution.

In a conventional heat transfer system, the heat transfer coefficient is calculated from the heat flux and the temperature difference between the hot wall and the bulk fluid. In the present study, the mass transfer coefficient was calculated from the mass flux (measured by the electric current) and the differences in the cupric ion concentrations at the cathode surface, C_s, and bulk, C_b. The bulk concentration C_b is the same as the $CuSO_4$ concentration. However, it is difficult to measure C_s. Thus, the limiting-current technique was used to determine the cupric ion concentration at the cathode surface. As the applied potential increased, the current between the electrodes increased for a while then reached a plateau region, where a further increase in the applied potential did not affect the current. This occurred because the process of cupric ion reduction at the cathode surface is much faster than that of cupric ion transfer from anode to cathode. The current at the plateau was termed the limiting current; at the limiting current value, the cupric ion concentration at the cathode surface can be treated as zero. The mass transfer coefficient, h_m, can be calculated from the bulk concentration, C_b, and the limiting current density, I_{lim}. The total mass-transfer flux due to diffusion, convection, and electric migration of cupric ions is given by I/nF. Among the flux, the mass-transfer flux due to electric migration, calculated by $t_{Cu^{2+}}/nF$, should be excluded as this process does not occur in the heat transfer system. With the limiting current, the mass-transfer coefficient becomes:

$$h_m = \frac{(1 - t_{Cu^{2+}})I}{nF(C_b - C_s)} = \frac{(1 - t_{Cu^{2+}})I_{lim}}{nFC_b}. \quad (15)$$

Further details of the experimental method can be found in the work of Ko et al. [16].

Table 1 – Dimensionless numbers for the analogous systems.

Heat transfer		Mass transfer	
Nusselt number	$\frac{h_h H}{k}$	Sherwood number	$\frac{h_m H}{D_m}$
Prandtl number	$\frac{\nu}{\alpha}$	Schmidt number	$\frac{\nu}{D_m}$
Rayleigh number	$\frac{g\beta\Delta TH^3}{\alpha\nu}$	Rayleigh number	$\frac{gH^3}{D_m\nu}\frac{\Delta\rho}{\rho}$

3.2. Oxide pool phenomena

The oxide pool is heated continuously by decay heat. The exterior wall of the reactor vessel is cooled by the ERVC system. The natural convection flow at the oxide pool is envisaged to descend along the inner surface of the bottom head by cooling, congregates at the center of the bottom head, and then rises and flows outward to the edges of the top plate. A number of natural convection flow cells are also formed underneath the top plate due to cooling by the top plate. In the mass transfer experiment using the electroplating system, the limiting current is measured at the cathode and the anode is not used because of the precipitation reaction at the anode surface [24]. At the cathode surface, a buoyancy force was induced because of a decrease in the cupric ion concentration and, hence, upward flow formation. To simulate the flow that descends along the inner surface of the lower head prior to congregating at the center of the bottom head, the gravitational direction has to be reversed. Thus, these experiments were performed using an inverted arrangement of the test rig as shown in Fig. 1C).

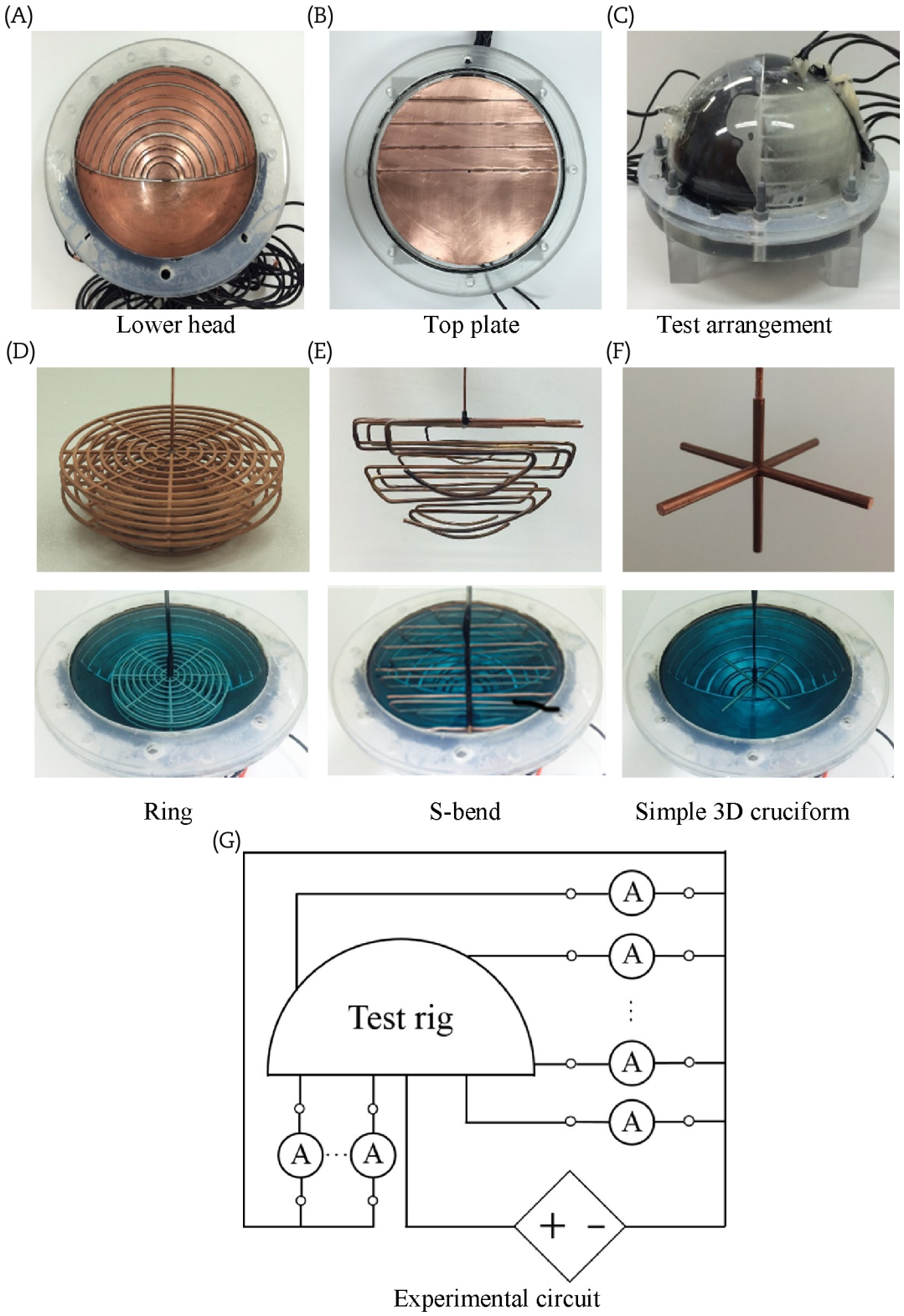

Fig. 1 – MassTER-OP3 and test arrangement. MassTER-OP3, Mass Transfer Experimental Rig for the three-dimensional Oxide Pool.

3.3. Similarity

The modified Rayleigh number (Ra'_H) was substituted for the well-known Rayleigh number (Ra_H) to describe the volumetric heat source:

$$Ra'_H = Ra_H \times Da = \frac{g\beta\Delta T H^3}{\alpha\nu} \times \frac{q''' H^2}{k\Delta T} = \frac{g\beta q''' H^5}{\alpha\nu k}, \quad (16)$$

where

$$Da = \frac{q''' H^2}{k\Delta T}, \quad \text{Damköler number.} \quad (17)$$

The heat flux (q), temperature (T), and thermal conductivity (k) of the heat transfer system correspond to the current (I), cupric ion concentration (C_{CuSO4}), and mass diffusivity (D_m), respectively, as shown in Table 2. Using Eq. (18), the mass transfer Damköler number, Da_m, can be expressed as:

$$Da_m = \frac{(1 - t_{Cu^{2+}}) I'''_{lim} H^2}{nFD_m C_b}. \quad (18)$$

Then

$$Ra'_{Hm} = Ra_H \times Da_m = \frac{gH^3\Delta\rho}{D_m\nu\rho} \times \frac{(1 - t_{Cu^{2+}}) I'''_{lim} H^2}{nFD_m C_b} = 128.5 \frac{(1 - t_{Cu^{2+}}) g I'''_{lim} H^5}{nFD_m^2 \nu\rho}, \quad (19)$$

where

$$\frac{\Delta\rho}{C_b} = \frac{\Delta\rho}{\Delta C} \sim 128.5. \quad (20)$$

3.4. Test rig

Fig. 1 shows the Mass Transfer Experimental Rig for the 3D Oxide Pool (MassTER-OP3) and the system circuit. MassTER-OP3 consists of a lower head, a top plate, and volumetric heat sources. Half of the lower head is a one-piece electrode, and the other half is segmented into nine piecewise electrodes; the top plate has a similar design. The local average mass fluxes were measured with the piecewise electrodes. Comparisons of the summation of the current measured by the piecewise electrodes with a one-piece electrode confirmed the accuracy of the rig. VüPower-K1205D was used as the power supply and a FLUKE-15B+ multimeter was connected to each electrode to measure the electric current.

As described in Section 3.1, a large buoyancy force is generated by a compact test rig using a copper electroplating system. Therefore, the Ra'_H of the MassTER-OP3 experiment was about 1,000 times larger than that of a heat transfer experiment with identical geometry. In this study, the height of the MassTER-OP3 was only 0.1 m. This corresponds to a Ra' of 10^{14} order, which varies depending on the electric current density.

Figs. 1D–1F show the volumetric heat sources. Table 1 lists their geometries. Two of them have configurations identical to those of SIGMA 3D [5] and LIVE [6], but they were linearly scaled. The other was designed by the authors to investigate the influence of volumetric heat sources. The total wire length of the ring heat source was more than two times longer than that of the S-bend heat source. The simple 3D cruciform heat source had an extremely short length. The wire electrode of the S-bend heat source was homogeneously distributed in the hemispherical space. The wire electrode of the ring heat source was much longer and was densely distributed in the lower part of the hemisphere.

3.5. Test matrix

Table 3 summarizes the test matrix. Three volumetric heat sources were compared. The lower head was isothermal in all cases. The top plate was either isothermal or adiabatic.

3.6. Uncertainty analyses

Uncertainties in the $CuSO_4$–H_2SO_4 mass transfer experiments were analyzed using data reduction methods [25]. Because the final dependent variable was the Sherwood number, data reduction and uncertainty can be expressed as:

$$Sh_H = \frac{h_m H}{D_m} \Rightarrow Sh_H = f(h_m, D_m, H)$$

and

$$U^2_{Sh_H} = \left(\frac{\partial Sh_H}{\partial h_m} U_{h_m}\right)^2 + \left(\frac{\partial Sh_H}{\partial D_m} U_{D_m}\right)^2 + \left(\frac{\partial Sh_H}{\partial H} U_H\right)^2, \quad (21)$$

where the uncertainties in h_m and H were estimated in the same way as in Eq. (21), until basic measurement quantities remained, i.e., the length, the masses of H_2SO_4 and $CuSO_4$, and the electric current. The uncertainties regarding the concentrations of H_2SO_4 and $CuSO_4$ were calculated using the above basic measurement quantities.

The measurement errors of the basic quantities were assumed to be half that of their smallest scales. The estimated errors in length, mass, and current measurement were 2.5×10^{-5} m, 5×10^{-7} kg, and 5×10^{-5} A, respectively. The calculated fractional average uncertainties were less than

Table 2 – Geometries of the anodes as volumetric heat sources.

	Length (mm)	Width (mm)	Height (mm)	Total wire length (mm)
Ring	134	134	46	7,552
S-bend	180	168	80	2,940
Simple 3D cruciform	100	100	80	275

3D, three-dimension.

Table 3 – Test matrix for experiments.

Volumetric heat source	Pool top	Ra'_H
Ring (LIVE)	Insulated	1.48×10^{14}
	Cooled	2.96×10^{14}
S-bend (SIGMA 3D)	Insulated	1.60×10^{14}
	Cooled	3.49×10^{14}
Simple 3D cruciform	Insulated	1.36×10^{14}
	Cooled	4.24×10^{14}

LIVE, Late In-Vessel phase Experiments; SIGMA 3D, Simulation of Internal Gravity-driven Melt Accumulation Three-Dimensional.

Table 4 – Comparison of electric current measured by one piece and segmented piecewise electrodes.

	Top cooled			Top insulated		
	Ring	S-bend	Simple 3D cruciform	Ring	S-bend	Simple 3D cruciform
Lower head	1.51	3.2	7.96	7.05%	1.21%	9.5
Top plate	10.25	7.72	2.73	–	–	–

Data are presented as %.
3D, three-dimension.

0.26%, which shows the inherent accuracy of the experimental technique. The largest uncertainties resulted from length measurement as it affects many parameters.

4. Results and discussion

4.1. Comparison of one-piece and piecewise electrodes

Table 4 compares the electric current measured by the one-piece electrode with the summation of those measured by the piecewise electrodes. The average measurement difference was about 5%; the maximum was about 10%. Thus, the influence of the thin insulated areas between piecewise electrodes was negligible.

4.2. Comparisons of the mean Nusselt numbers

Fig. 2 shows the measured *Sh*'s, which correspond to *Nu*'s in a heat transfer system. It compares the *Nu*'s with the previously reported studies. The Nu_{dn} measured by the MassTER-OP3 was about 30% lower than that previously reported. The difference was caused either by the experimental method or by the experimental difficulties with the heat transfer measurement, such as heat leakage or radiation heat transfer. Our test results were close to those of ACOPO. An ice crust was formed inside the pool because of the extremely low coolant temperature (−80°C) in the BALI experiment. ACOPO, a quasi-stationary experiment, used a preheated working fluid as a volumetric heat source.

Fig. 2A shows that the influence of the heat sources does not appear in the Nu_{dn} values. The Nu_{up} values reported previously and produced by MassTER-OP3 were scattered. Fig. 2B clearly shows the influence of the volumetric heat sources. The Nu_{dn} for the simple 3D cruciform case was the highest, followed by the S-bend and ring heat sources. The Nu_{up} of the ring case shows only a 1% difference with the existing natural convection correlation (22) for the upward facing hot surface condition [9].

$$Nu_L = 0.15Ra_L^{1/3}, \quad \text{where } L = \frac{A}{p}. \tag{22}$$

The natural convection on the hot plate and that beneath the cold plate are phenomenologically the same. Thus, natural convection beneath the top plate was unaffected by the main natural convective flow occurring at the lower head; this was attributed to the relatively large friction loss for the rising flow from the bottom because of the densely spaced wire electrodes of the ring case. Thus, it may be concluded that Nu_{dn} is unaffected by the structure of the wire heat source, whereas Nu_{up} is affected.

4.3. Comparison of local heat transfer

Fig. 3 compares the measured angular heat transfer coefficient ratios with those from LIVE using a ring heat source. The Ra'_H

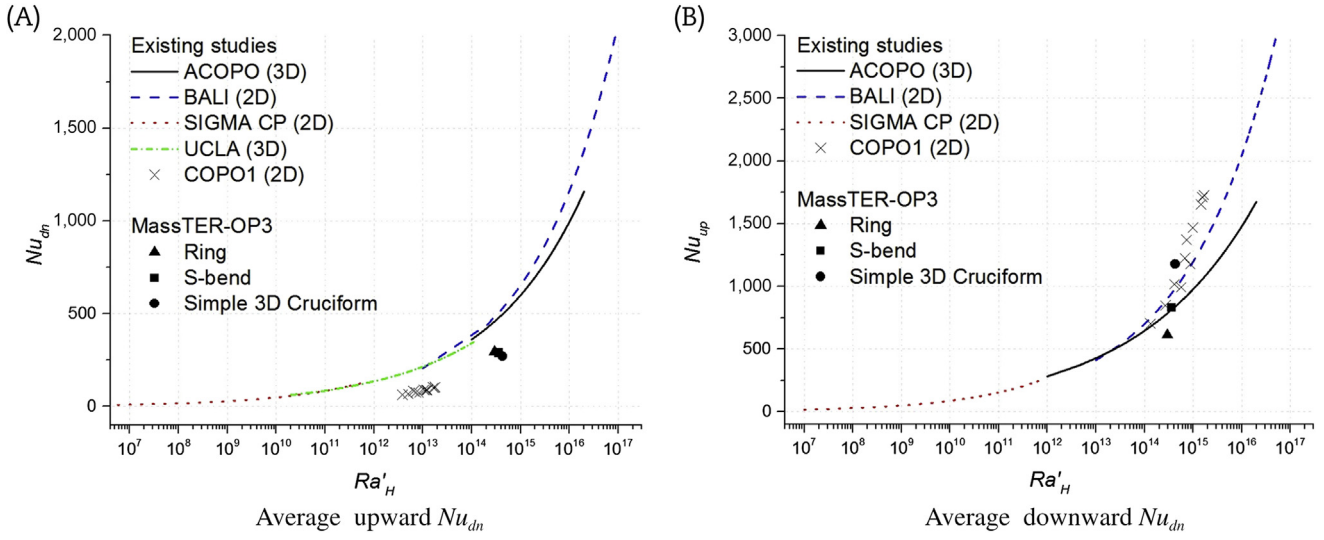

Fig. 2 – Comparisons of the *Nu*'s with the existing studies. 2D, two-dimension, 3D, three-dimension.

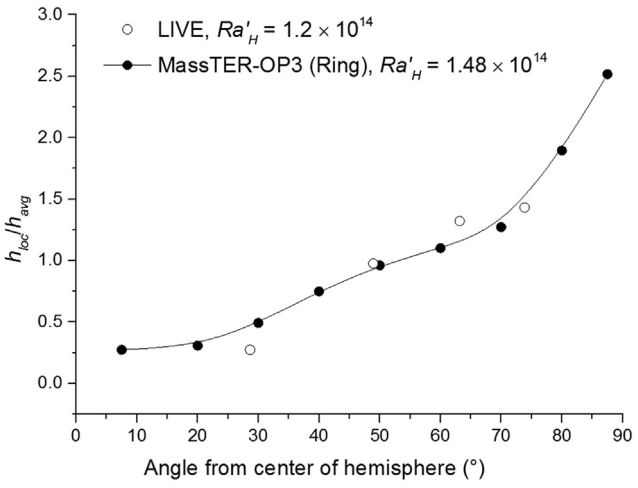

Fig. 3 – A comparison of angular heat transfer coefficient ratios with LIVE cases. LIVE, Late In-Vessel phase Experiments.

was about 10^{14} in both cases. The heat flux increased with the angle in both cases and had similar slopes. The curve shows a sharp increase at 70°. This seems to be caused by the leading edge effect and thickening of the boundary layer due to the flow that gathers near the bottom. However, the heat flux above 77° was not measured in the LIVE experiment.

Fig. 4 compares the measured angular heat transfer coefficient ratios of MassTER-OP3 with those from the SIGMA 3D experiment using an S-bend heat source. The Ra'_H values of the SIGMA 3D and MassTER-OP3 experiments were about 10^{10} and 10^{14}, respectively. The heat flux increased with the angle in both cases. However, the heat flux increased steadily up to 90° for MassTER-OP3, whereas for SIGMA 3D it showed a peak in the vicinity of 80°. The subsequent fall in the heat flux can be explained by the influence of the flow under the top plate. The overlapped boundary layers in the top corner resulted in a fall in the heat flux in the top position. Fig. 5 shows the two steady-state temperature fields calculated by FLUENT 6.3 for the 2D case. The Ra'_H was about 10^{14}, and *Pr* was 2 and 2,014, respectively, which correspond to *Sc* in the mass transfer experiments. The overlapped boundary layers were thick for a low *Pr*. Thus, the peak value and subsequent fall in the heat flux may be attributed to the relatively thick overlapped boundary layer of the SIGMA 3D experiment.

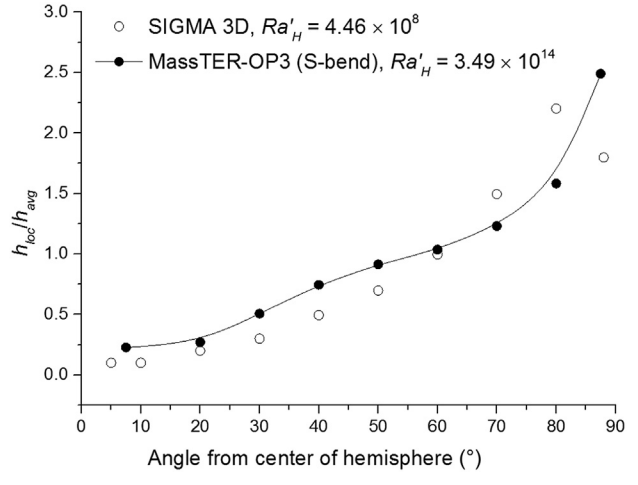

Fig. 4 – A comparison of angular heat transfer coefficient ratios with SIGMA 3D cases. SIGMA 3D, Simulation of Internal Gravity-driven Melt Accumulation Three-Dimensional.

Fig. 6 compares the local heat transfer coefficient ratio of the top plate with respect to the position from SIGMA 3D and MassTER-OP3. The local heat flux was scattered for the S-bend heat source, but was nearly constant for the ring heat source. LIVE used an insulated top plate and did not measure the Nu_{up}'s. The rising flows in the hemisphere pool of SIGMA 3D and MassTER-OP3 (S-bend) had similar characteristics because of the similar geometry of their volumetric heat sources. Therefore, the measured Nu_{up}'s were similar. The Nu_{up} of the MassTER-OP3 (ring) experiment was similar to that from the natural convection heat transfer correlation (22) on the horizontal hot plate, which was unaffected by other flows. The Nu_{up} of the simple 3D cruciform heat source displayed a decreasing trend with radial position. The highest Nu_{up} was measured because of the rising flow at the center.

Fig. 7 compares the angular heat transfer coefficient ratios of the UCLA and MassTER-OP3 experiments for both isothermal and adiabatic top plate cooling conditions. The heat fluxes measured by MassTER-OP3 were similar regardless of the difference in the top cooling conditions. By contrast, the fluxes measured by UCLA were similar but not identical. The peak was formed at a higher position in the adiabatic top condition than in the isothermal top condition. This may also be explained by the formation of an overlapped boundary layer in the top corner. The cooled top plate formed a natural convective boundary layer and, as a result, the overlapped boundary layer was thickened. A comparison of SIGMA 3D and UCLA confirmed that the *Pr* of the UCLA experiment (working fluid: Freon-113) was about 3, and the peak formed at a higher position than in SIGMA 3D (working fluid: water).

5. Conclusions

We investigated natural convection heat transfer from an oxide pool to a reactor vessel using the mass transfer experimental method based on the analogy between heat and mass transfer (MassTER-OP3). For a 3D hemisphere experimental facility, the local average mass fluxes were measured using piecewise electrodes. Owing to the limitations of the experimental method, a cathode was used for the measurement, and MassTER-OP3 tests were conducted in an inverted arrangement to change the direction of gravitation.

The influence of the simulated volumetric heat sources was compared by adopting similar wire heat sources for SIGMA 3D, LIVE, and simple 3D cruciform. Ra'_H and *Pr* were on the order of 10^{14} and 2,014, respectively. Isothermal conditions were established for the lower head; isothermal and adiabatic conditions were established for the top plate.

The measured Nu_{dn}'s were ~30% lower than those previously reported, but the MassTER-OP3 results were similar

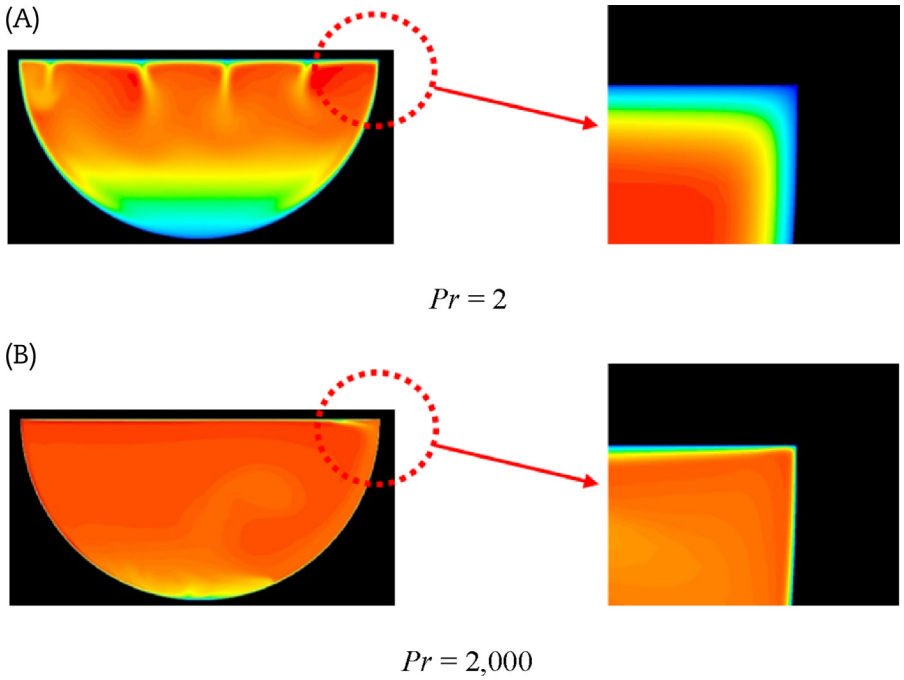

Fig. 5 – Calculated temperature field for Ra'_H ~10^{14}.

regardless of the type of volumetric heat source and top cooling conditions. The angular heat transfer coefficient ratios were also similar. However, peaks that appeared near the top position owing to overlapped boundary layers were not measured because of the high *Pr* value of the MassTER-OP3 experiments.

The different volumetric heat sources did not have an effect on the angular heat fluxes along the lower head; however, the heat fluxes of the top plate were affected by the heat sources. The long, densely distributed wire heat source obstructed the rising flow from the bottom; as a result, the Nu_{up} values measured at the top plate were close to that of the natural convection heat transfer correlation (22) of a hot horizontal plate for a ring heat source.

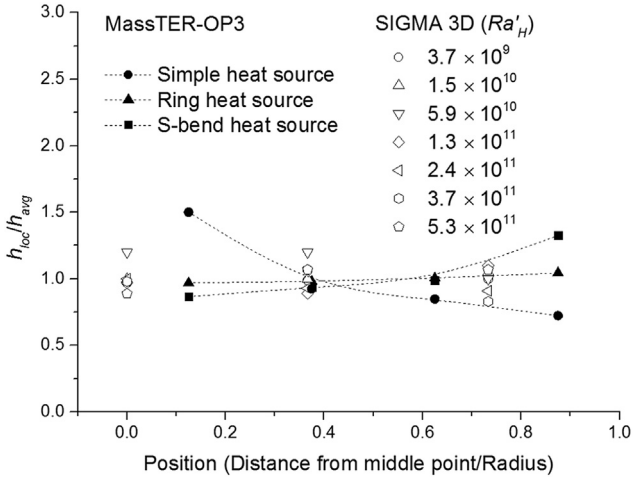

Fig. 6 – A comparison of heat transfer coefficient ratio between mass transfer and SIGMA 3D experiment with respect to radial position. SIGMA 3D, Simulation of Internal Gravity-driven Melt Accumulation Three-Dimensional.

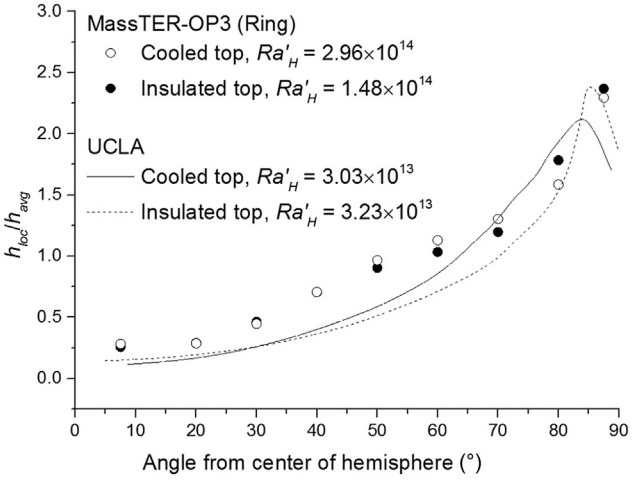

Fig. 7 – Comparison of heat transfer coefficient ratios of MassTER-OP3 (Ring) and UCLA experiments with respect to top plate cooling conditions. MassTER-OP3, Mass Transfer Experimental Rig for the Three-Dimensional Oxide Pool.

Conflict of interest

There is no conflict of interest with any financial organization regarding the material discussed in the manuscript.

Acknowledgments

This study was sponsored by the Ministry of Science, Information, Communication and Technology (ICT) & Future

Planning (MSIP), and was supported by a Nuclear Research & Development program grant funded by the National Research Foundation (NRF; Grant code: 2014M2A8A1030777).

Nomenclature

A	area [m^2]
C	molar concentration [kmol/m^3]
D_m	mass diffusivity [m^2/s]
Da	Damköler number ($q'''H^2/k\Delta T$)
F	Faraday constant [96,485,000 Coulomb/kmol]
g	gravitational acceleration [9.8 m/s^2]
Gr_H	Grashof number ($g\beta\Delta TH^3/\nu^2$)
h	heat transfer coefficient [W/m^2·K]
h_m	mass transfer coefficient [m/s]
H	height [m]
I_{lim}	limiting current density [A/m^2]
k	thermal conductivity [W/m·K]
L	characteristic length of the plane surface (A/p)
n	number of electrons in charge transfer reaction
Nu_H	Nusselt number (h_hH/k)
p	wetted perimeter (m)
Pr	Prandtl number (ν/α)
Ra_H	Rayleigh number ($GrPr$)
Ra'_H	modified Rayleigh number ($RaDa$)
Sc	Schmidt number (ν/D_m)
Sh_H	Sherwood number (h_mH/D_m)
T	temperature (K)
t_n	transference number
U_x	uncertainty of x

Greek symbols

α	thermal diffusivity (m^2/s)
β	volume expansion coefficient (1/K)
γ	dispersion coefficient
μ	viscosity (kg/m·s)
ν	kinematic viscosity (m^2/s)
ρ	density (kg/m^3)

Subscripts

b	bulk
dn	lower head
h	heat transfer system
m	mass transfer system
up	top plate

REFERENCES

[1] J.M. Bonnet, J.M. Seiler, Thermal hydraulic phenomena in corium pools: the BALI experiment, in: 7th International Conference on Nuclear Engineering, Tokyo, Japan, 1999.

[2] O. Kymalainen, H. Tuomisto, O. Hongisto, T.G. Theofanous, Heat flux distribution from a volumetrically heated pool with high Rayleigh number, Nucl. Eng. Des. 149 (1994) 401–408.

[3] B.R. Sehgal, V.A. Bui, T.N. Dinh, J.A. Green, G. Kolb, SIMECO Experiments on in-vessel melt pool formation and heat transfer with and without a metallic layer, in: Proceedings of In-Vessel Core Debris Retention and Coolability Workshop, Garching, Germany, 1998, pp. 205–213.

[4] J.K. Lee, K.Y. Suh, K.J. Lee, J.I. Yun, Experimental study of natural convection heat transfer in a volumetrically heated semicircular pool, Ann. Nucl. Energy 73 (2014) 432–440.

[5] K.Y. Suh, et al., In-vessel Retention Strategy for High Power Reactors, Korea Electrical Engineering & Science Research Institute, Korea, 2005.

[6] A. Palagin, F. Kretzschmar, LIVE test FSt4: experimental results and simulation by CONV code, in: 13th International Topical Meeting on Nuclear Reactor Thermal Hydraulics, Kanazawa City, Japan, 2009.

[7] F.J. Asfia, V.K. Dhir, An experimental study of natural convection in a volumetrically heated spherical pool bounded on top with a rigid wall, Nucl. Eng. Des. 163 (1996) 333–348.

[8] T.G. Theofanous, M. Maguire, S. Angelini, T. Salmassi, The first results from the ACOPO experiment, Nucl. Eng. Des. 169 (1997) 49–57.

[9] A. Bejan, Convection Heat Transfer, fourth ed., Wiley & Sons, New Jersey, 2003.

[10] V.G. Levich, Physicochemical Hydrodynamics, Prentice-Hall, Englewood Cliffs, New Jersey, 1962.

[11] J.N. Agar, Diffusion and convection at electrodes, Discuss. Faraday Soc. 26 (1947) 27–37.

[12] C.W. Tobias, R.G. Hickman, Ionic mass transfer by combined free and forced convection, Int. J. Res. Phys. Chem. Chem. Phys. 229 (1965) 145–166.

[13] E.J. Fenech, C.W. Tobias, Mass transfer by free convection at horizontal electrodes, Electrochim. Acta 2 (1960) 311–325.

[14] J.H. Heo, B.J. Chung, Natural convection heat transfer on the outer surface of inclined cylinders, Chem. Eng. Sci. 73 (2012) 366–372.

[15] M.S. Chae, B.J. Chung, The effect of pitch-to-diameter on natural convection heat transfer of two vertically aligned horizontal cylinders,, Chem. Eng. Sci. 66 (2011) 5321–5329.

[16] S.H. Ko, D.W. Moon, B.J. Chung, Applications of electroplating method for heat transfer studies using analogy concept, Nucl. Eng. Technol. 38 (2006) 251–258.

[17] K.U. Kang, B.J. Chung, The effects of the anode size and position on the limiting currents of natural convection mass transfer experiments of natural convection mass transfer experiments in a vertical pipe, Trans. KSME(B) 34 (2010) 1–8.

[18] J.H. Heo, B.J. Chung, Influence of helical tube dimensions on open channel natural convection heat transfer, Int. J. Heat Mass Transfer 55 (2012) 2829–2834.

[19] J.Y. Moon, B.J. Chung, Time-dependent Rayleigh–Benard convection: cell formation and Nusselt number, Nucl. Eng. Des. 274 (2014) 146–153.

[20] M.S. Chae, B.J. Chung, Natural convection heat transfer in a uniformly heated horizontal pipe, Heat Mass Transfer 50 (2014) 114–123.

[21] H.K. Park, B.J. Chung, Optimal tip clearance in the laminar forced convection heat transfer of a finned plate in a square duct, Int. Commun. Heat Mass Transfer 63 (2015) 73–81.

[22] J. Krysa, A.A. Wragg, D.M. Thomas, M.A. Patrick, Free convection mass transfer in open upward-facing cylindrical cavities, Chem. Eng. J. 79 (2000) 179–186.

[23] J. Krysa, D. Houf, C.F. Oduoza, A.A. Wragg, Free convective mass transfer at up-pointing truncated cones, Chem. Eng. J. 85 (2002) 147–151.

[24] Y. Konishi, Y. Nakamura, Y. Fukunaka, K. Tsukada, K. Hanasaki, Anodic dissolution phenomena accompanying supersaturation of copper sulfate along a vertical plane copper anode, Electrochim. Acta 48 (2003) 2615–2624.

[25] W.G. Steele, H.W. Coleman, Experimental and Uncertainty Analysis for Engineers, second ed., John Wiley & Son, Canada, 1999.